Unusual magnetotransport properties in a FeAs single crystal

Seunghyun Khim,[1,*] Matthias Gillig,[1] Rüdiger Klingeler,[2] Sabine Wurmehl,[1,3] Bernd Büchner,[1,3] and Christian Hess[1,4]
[1]*Leibniz-Institute for Solid State and Materials Research, Helmholtzstraße 20, 01069 Dresden, Germany*
[2]*Kirchhoff Institute of Physics, Heidelberg University, 69120 Heidelberg, Germany*
[3]*Institut für Festkörperphysik, TU Dresden, 01062 Dresden, Germany*
[4]*Center for Transport and Devices, TU Dresden, 01069 Dresden, Germany*
(Received 21 October 2015; revised manuscript received 4 May 2016; published 16 May 2016)

We have investigated the magnetoresistance (MR) and Hall resistivity properties of a FeAs single crystal which exhibits magnetic order below $T_N = 69$ K. We observe nonlinear Hall resistivity and linear MR in the presence of magnetic-order-connected Fermi surface reconstruction. The analysis of the magnetotransport data using a two-carrier model suggests the emergence of an additional minor hole Fermi surface which coexists with major electron carriers below T_N. The origin of the linear MR, however, remains inconsistent with current explanations based on the electronic band structure, i.e., the quantum linear MR model from linearly dispersive Dirac cones and linear MR as a result from strong velocity changes of the cyclotron motion near nested Fermi surfaces. While a macroscopic inhomogeneity in a mobility distribution may cause the linear MR as widely observed in other semimetals with high mobilities, the spiral magnetic order of FeAs seems to ask for an alternative description which takes the specific magnetic order and details of the electronic structure of FeAs as well as a possible entanglement between them into account.

DOI: 10.1103/PhysRevB.93.205129

I. INTRODUCTION

Interaction between noncollinear magnetic order and itinerant electrons has recently come into focus as the source of new quantum phenomena. A prominent representative material is MnSi with the cubic B20 structure lacking inversion symmetry. Here, competition between Dzyaloshinskii-Moriya (DM) interaction and Heisenberg exchange interaction leads to a helical spin ground state [1,2]. More interestingly, an exotic spin texture, the so-called Skyrmion state, emerges close to the helical phase in a finite-field range. The spin-helical and the Skyrmion states have attracted much attention due to emergent quantum phenomena originating from an entanglement between the local (or topological) moment and itinerant electrons [3,4].

The binary transition-metal compounds with a MnP-type structure, such as MnP, CrAs, FeP, and FeAs, also possess a noncollinear spin spiral order [5–9]. In this class of materials, the competing interaction via indirect Ruderman-Kittel-Kasuya-Yosida (RKKY) exchange and Fermi surface nesting were discussed as a possible origin of the spiral magnetic order. One remarkable feature is their appearance of superconductivity under pressure in CrAs ($T_c \sim 2.2$ K at 1 GPa) and MnP ($T_c \sim 1$ K at 8 GPa) when the magnetic order is suppressed [10–12]. Their phase diagrams feature a domelike superconducting phase after a gradual suppression of the magnetic phase. This is reminiscent of the phase diagrams of cuprates, heavy fermions, and iron-based superconductors [13]. Non-Fermi-liquid behavior evidenced in resistivity implies the existence of a quantum critical point (QCP), and spin fluctuations are accordingly considered to play a decisive role in inducing the superconducting instability [10,11]. However, neutron diffraction and nuclear magnetic resonance (NMR) experiments identified a first-order nature of the magnetic transition, contradicting the QCP scenario [14,15].

FeAs, however, does not show superconductivity under pressure up to 50 GPa [16]. A neutron scattering experiment identified an incommensurate spiral spin-density wave (SDW) with a second-order nature below $T_N = 69$ K. The ordered magnetic moments whose magnitude is $\sim 0.5\mu_B$/Fe are confined on the (101) plane and propagate along the [010] direction with the propagating vector $\mathbf{q} = 0.38\mathbf{b}^* – 0.4\mathbf{b}^*$ at 4 K [8,17]. The absence of superconductivity in FeAs under pressure seems to be rather interesting because the layered FeAs lattice of the iron-based superconductors undergoes a SDW transition as well, and the magnitude of the magnetic moment is similar to that of FeAs.

While the magnetic structure of FeAs has been intensively investigated by the neutron scattering experiments, little information is available for detailed transport properties of FeAs. In this paper we present the magnetotransport properties of FeAs. When the magnetic order is developed below T_N, we observe a deviation of the magnetoresistance (MR) from a conventional quadratic magnetic field dependence, whereas that of the Hall resistivity becomes nonlinear. We discuss these anomalous transport behaviors with a close interplay between the magnetic order and the itinerant electrons as well as possible spatial inhomogeneity in carrier mobility.

II. EXPERIMENT

Single-crystalline FeAs was grown by the chemical-vapor-transport method using iodine as the transport agent. Prereacted FeAs powder and iodine pieces were sealed inside an evacuated quartz tube and heated for a week in a two-zone furnace in which hot- and cold-zone temperatures were kept at 900°C and 700°C, respectively. The chemicals were placed in the hot zone, and the grown single crystals were found in the cold zone. We confirmed the composition of the FeAs single crystals by using an energy dispersive x-ray spectroscopy (EDX) analysis. The crystal structure was confirmed by x-ray diffraction to be orthorhombic (space group *Pnma*). The

*Seunghyun.Khim@cpfs.mpg.de

obtained lattice parameters are $a = 5.423$ Å, $b = 6.008$ Å, and $c = 3.363$ Å, which are consistent with previously reported values.[7]

For the transport measurement, the FeAs single crystal oriented by Laue x-ray diffraction was polished into a bar shape, and copper wires were attached on the sample using silver paste. The longitudinal and Hall resistivity were measured by using a conventional five-probe method. For zero-field measurements the longitudinal resistivity was measured along all principal axes, while for magnetotransport, a 5-mA excitation current was applied along the [001] direction and the magnetic field was applied along the [100] direction. The Hall voltage was measured across the [010] direction. We removed an offset of the Hall voltage by symmetrizing data measured on a positive- and negative-field sweep. As a result the Hall resistivity is given as $\rho_{xy}(H) = [\rho_{xy}(+H) - \rho_{xy}(-H)]/2$.

III. RESULTS AND DISCUSSION

We plot in Fig. 1(a) the zero-field temperature-dependent resistivity curves measured along three different directions. At high temperatures above 200 K, the resistivity is anisotropic. Not only are the resistivity values highly different, but the signs of the resistivity slope on temperature are not identical for the different directions. The curves for the [100] and [010] directions display a metallic character ($d\rho/dT > 0$), while the curves for the [001] direction show the opposite ($d\rho/dT < 0$). This observation is consistent with previous findings [18]. As the crystal structure of FeAs does not show any low-dimensional character like a well-defined layer or chain structure, the resistivity anisotropy in the high temperature is unusual. At the magnetic ordering temperature, $T_N = 69$ K, a clear drop occurs, and the resistivity further decreases upon lowering the temperature for all crystallographic directions. The resistivity values subsequently become similar, in contrast to the anisotropic high-temperature behavior.

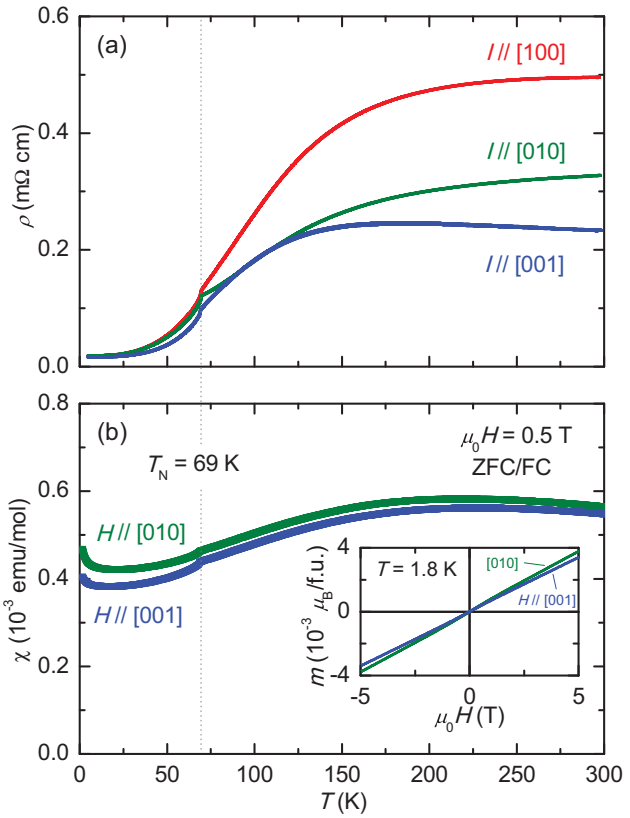

FIG. 1. (a) Temperature dependence of resistivity ρ for the three crystallographic directions in zero field. (b) Temperature dependence of the magnetic susceptibility under $\mu_0 H = 0.5$ T along the [010] and [001] directions. Inset: Field dependence of the magnetization at $T = 1.8$ K.

We plot in Fig. 1(b) the temperature-dependent magnetic-susceptibility curves along the [010] and [001] directions. The data obtained in field-cooled (FC) and zero-field-cooled (ZFC) measurements do not show a noticeable difference. This observation is contradictory to the previous report showing a bifurcation between the ZFC and FC curves for the [001] direction [18]. Above T_N, neither curve follows the Curie-Weiss relation, but a broad maximum is present around ~220 K [8]. The curves show a sharp drop at T_N consistent with the resistivity data. The fact that the size of the drop across T_N is slightly larger for the [001] direction than that for the [010] direction would be in accordance with the two-dimensional character of the spin-spiral order. However, the weak anisotropy in susceptibility below T_N seems to be rather unusual in terms of the spin-spiral order [8,17]. This probably means that a paramagnetic contribution from itinerant electrons would dominate the magnetic susceptibility. The magnetization has a monotonic field dependency, indicating no abrupt change in the magnetic order or in the electronic structure up to 5 T [see the inset of Fig. 1(b)].

It should be pointed out that the properties of FeAs above T_N are not ascribed to a conventional paramagnetic metal. The resistivity along the [001] direction shows semiconductorlike behavior, and the magnetic susceptibility shows a non-Curie-Weiss relation. Together with the strongly temperature dependent R_H, which will be discussed below, these observations suggest a large population change in states close to the Fermi level by thermal activation like in a narrow-band-gap semiconductor [8,19]. It reflects the complex electronic structure of FeAs where five of the iron d orbitals may, in general, contribute in a comparable manner to the states near the Fermi level [20].

In order to investigate a coupling between spin and charge degrees of freedom, we have measured the resistivity under different magnetic fields. We plot in Fig. 2 the field-dependent MR curves, with MR $= [\rho(H) - \rho(0\text{T})]/\rho(0\text{T})$. MR is nearly negligible above 100 K, but it continuously increases with decreasing temperature, reaching 50% at 10 K and upon 15 T. Its curvature also evolves with temperature. While the curves are quadratic above T_N [Fig. 2(b)], the linear MR appears at high fields upon cooling below T_N. As shown in the data at 10 K, the quadratic MR persisting to 3 T smoothly turns to the linear MR, which is also featured as a plateau in the field derivative curves ($d\rho/dT$) above 10 T (the inset of Fig. 2). The quadratic MR region expands to higher fields as temperature increases. As this behavior is apparently developed in the magnetically ordered state, this suggests a finite coupling between the magnetic order and charge transport.

The Hall measurement introduces additional information on the charge transport. We show in Fig. 3 the field-dependent

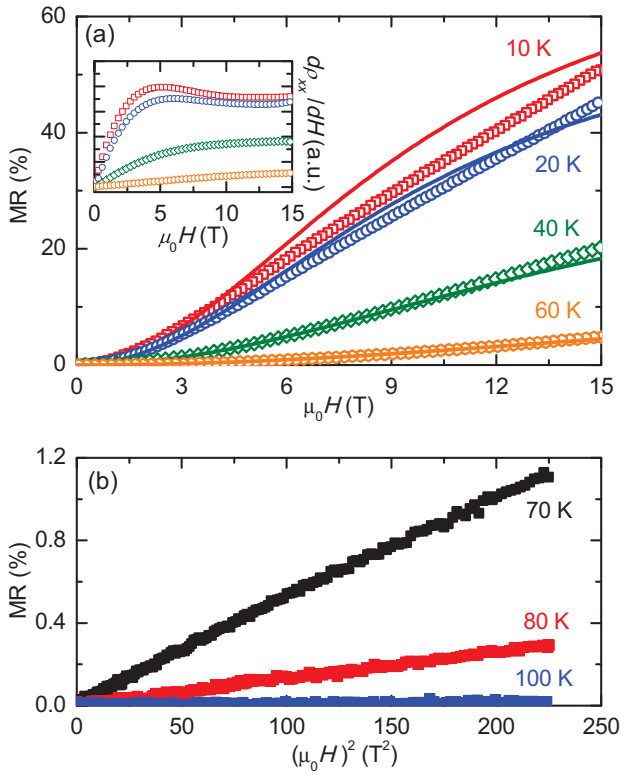

FIG. 2. (a) Field dependence of the magnetoresistance (MR) measured at 10, 20, 40, and 60 K. The solid lines represent the two-band model fitting curves based on Eq. (2). Inset: Corresponding field derivatives curves. (b) MR versus $(\mu_0 H)^2$ at 70, 80, and 100 K.

ρ_{xy} curves. The overall sign of ρ_{xy} is negative, suggesting that electron carriers dominate the transport. Above T_N, we observe a strong temperature dependency of the Hall coefficient, $R_H = \rho_{xy}/(\mu_0 H)$, where μ_0 is the permeability of free space, decreasing with temperature. Below T_N, the low-field R_H is nearly temperature independent. Instead, the slope of the

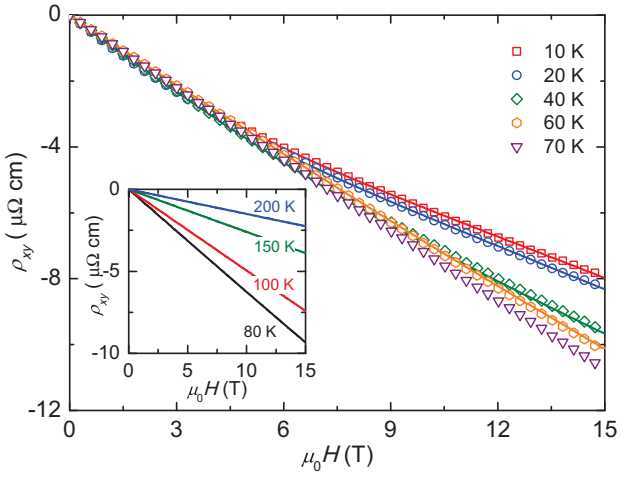

FIG. 3. Field dependence of the Hall resistivity ρ_{xy} measured at 10, 20, 40, 60, and 70 K. The solid lines represent the fitting curves within the two-carrier model written as Eq. (1). Inset: ρ_{xy} curves measured above T_N at 80, 100, 150, and 200 K.

ρ_{xy} curve is changed above 5 T, and this feature is gradually enhanced as temperature decreases. As a result, the nonlinear ρ_{xy} is clearly seen in the 10 K data.

In a ferromagnetic metal, the anomalous Hall effect should be taken into account in the analysis of the transport properties. As FeAs can be classified as an itinerant antiferromagnet with a small local magnetic moment, we expect a very weak anomalous Hall effect. The nonlinear ρ_{xy} can be alternatively attributed to the multiband character of FeAs. The onset of the magnetic order imposes an additional periodicity on the system, leading to Fermi surface reconstruction. As a consequence, additional Fermi surfaces can emerge. Within the multiband model, the reduction of the ρ_{xy} slope at high fields should be attributed to the presence of a minor hole carrier, while the overall negative sign proclaims a major electron carrier. For a qualitative analysis we introduce the empirical two-carrier model assuming that the complex electronic structure could be simplified into each representative electron and hole pocket [21]. The validity of the application of the phenomenological two-carrier model is supported by previous experimental results [9,18]. And the band calculation result showed that the Fermi surface structure of the antiferromagnetic ordered state consists of an electron pocket at the center of the Brillouin zone and four additional hole pockets in an intermediate region [20].

We try to fit both of the ρ_{xy} and MR curves using a single set of parameters, including densities and mobilities of hole and electron carriers at each temperature. According to this model, the field-dependent ρ_{xy} is written as

$$\rho_{xy} = \frac{\mu_0}{e}\frac{(\mu_h^2 n_h - \mu_e^2 n_e) + (\mu_h\mu_e)^2(n_h - n_e)(\mu_0 H)^2}{(\mu_e n_h + \mu_h n_e)^2 + (\mu_h\mu_e)^2(n_h - n_e)^2(\mu_0 H)^2} H, \tag{1}$$

where e is the electron charge and μ_h (μ_e) and n_h (n_e) are the mobility and density for the hole (electron) carrier. In parallel, MR is expressed as

$$\mathrm{MR} = \frac{\sigma_h\sigma_e(\mu_h + \mu_e)(\mu_0 H)^2}{(\sigma_h - \sigma_e)^2 + (\sigma_h\mu_e + \sigma_e\mu_h)^2(\mu_0 H)^2}, \tag{2}$$

where σ_h (σ_e) is the conductivity of the hole (electron) carrier. Assuming the Drude relation, $\sigma_i = e\mu_i n_i$ ($i = h,\ e$), the parameter set of (μ_h, μ_e, n_h, and n_e) can describe both ρ_{xy} and MR simultaneously. While we fitted the ρ_{xy} data up to 15 T, we only fitted the MR data below 3 T, showing the quadratic field dependency because the liner MR feature in the high fields is not compatible with the two-carrier model in which the MR should be saturated at high fields. We will discuss a possible origin of the linear MR feature later.

The resultant fitting curves well reproduce the corresponding experimental data, as shown in Figs. 2(a) and 3 for MR and ρ_{xy}, respectively. We plot the corresponding fitting parameters, carrier densities, and mobilities as a function of temperature in Fig. 4. For the data above T_N, we applied the single-band model to extract the carrier density and mobility for the dominating electron carriers. As described in the qualitative discussion, the two-carrier analysis captured the emergence of the hole carrier below T_N with a much smaller carrier density than n_e. Remarkably, n_h increases as temperature decreases in proportion to the development of the nonlinear feature in

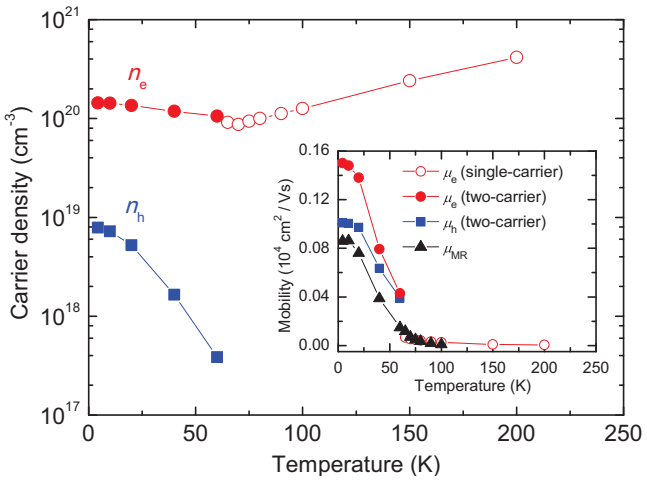

FIG. 4. Evolution of the carrier density with temperature. The values below T_N (solid symbols) were obtained from the two-band model analysis. Above T_N, the carrier density was calculated from the Hall coefficient. Inset: Mobility values retrieved from the single-, two-carrier model and the quadratic coefficients of MR.

ρ_{xy}. The temperature dependency of n_e is less pronounced, as reflected by the small change in the low-field R_H with temperature.

As shown in the inset of Fig. 4, the mobilities of both carriers progressively grow up below T_N. In contrast to the large difference in their carrier densities, the mobility of the electron carrier is only slightly larger than that of the hole carriers. Using an independent approach, we can extract an MR mobility μ_{MR} from the quadratic coefficient A of MR where $\mathrm{MR} = A(\mu_0 H)^2$ holds at low fields [22].

$$A = \frac{\sqrt{\sigma_e \sigma_h}}{\sigma_h + \sigma_e}(\mu_h + \mu_e) = \mu_{\mathrm{MR}} \leqslant \frac{1}{2}(\mu_h + \mu_e). \qquad (3)$$

This relation provides μ_{MR} as a lower bound of the average mobility of the two carriers. In our result the obtained μ_e and μ_h are both larger than μ_{MR}. This consistency implies that the mobilities obtained by two-carrier analysis are reasonable.

The dramatic change in the hole carrier density with temperature below T_N deserves further attention. We conjecture that this might be related to the temperature-dependent modulation vector of the spiral SDW order observed in the neutron scattering experiment [17] because the Fermi surface reconstruction is manipulated by the periodicity of the magnetic order. Thus, the gradual change in the modulation vector is likely to lead to a continuous modification in the electronic structure. It should be noted that the modulation vector is nearly constant below 20 K and the obtained transport parameters also seem to follow a similar trend. This coincidence could indicate the close relation between the transport properties and the underlying magnetic structure.

After having completed the rather conventional analysis of the low-field magnetotransport, we now move on to a discussion of the unusual MR at higher magnetic fields. The linear MR cannot be explained within a conventional multiband scenario. This failure has been shown in many different classes of materials [23]. One of the explanations is the linearly dispersive Dirac cone contribution to a magnetotransport. This is based on the so-called Abrikosov quantum linear MR model [24]. For instance, the linear MR in the $BaFe_2As_2$ was attributed to the constituent Dirac-cone structures, which are driven by the a hybridization between hole and electron pockets through the SDW order [22,25–27]. Despite the lack of direct evidence of a Dirac cone in FeAs, this scenario could be plausible for FeAs as this system also has SDW order upon the metallic electronic structure. The realization of the quantum linear MR requires a stringent condition that all carriers associated with the Dirac cone should occupy the lowest Landau level as an extreme quantum limit. To reach the extreme quantum limit in a relatively small field, the Fermi surface of the Dirac cone should be tiny, and the corresponding carrier density should be low. Moreover such a small pocket needs to dominate the magnetotransport properties over the other contributions from conventional bands. Applying this criterion to FeAs, the observed carrier densities are nearly two orders of magnitude larger than that in Ref. [24], where a crossover field of similar magnitude (2 T) corresponds to a carrier density $n \sim 10^{17}$ cm^{-3}. However, despite this inconsistency, we cannot completely rule out the possible existence of small Fermi surfaces that cannot be captured by the two-carrier analysis.

As an alternative scenario, it has been claimed that the linear MR could be a universal feature among materials that display the SDW magnetic order [28]. By the onset of the SDW order, the Fermi surface is mainly modified at the point where two separated bands hybridize due to the Fermi surface folding, leading to a partial gap opening. The remaining reconstructed Fermi surface possesses sharp turning points where the velocity of the carriers drastically changes in motion. At this point, the normal orbital motion of the carriers under an external magnetic field is disrupted, producing at low field an increased quadratic MR and above a crossover magnetic field (B^*) linear magnetoconductivity [28]. One might attempt to explain the linear MR in FeAs also within this scenario. In this case, B^* is proportional to Δ_m/τ, where Δ_m is the SDW gap and τ is the scattering time. As both Δ_m and τ usually increase with decreasing temperature, the temperature dependency of B^* is not trivial. However, upon Δ_m vanishing close to T_N, it should lead to $B^* \to 0$, and the linear MR accordingly should start to appear in a low field. In FeAs, while it is hard to explicitly determine B^* due to the broad curvature change in the MR data, B^* apparently increases with temperature. Furthermore, the MR curvature near T_N is quadratic, indicating a finite B^*. These observations are inconsistent with the expectation of this scenario.

As the linear MR behavior is widely observed among semimetals with high mobilities, a macroscopic spatial fluctuation in the mobility was suggested to induce the linear MR [29–32]. This model claims that the large spatial fluctuations produced by inhomogeneities lead to cycloidal trajectories in electron motion around low-mobility islands and result in linear MR. This scenario was experimentally evidenced, for instance, in doped Cd_3As_2 single crystals showing nonsaturating linear MR up to 65 T [32]. In FeAs, B^* increasing with temperature is consistent with this explanation in which B^* is proportional to the inverse of the carrier mobility. The mobility inhomogeneity could have been introduced during crystal growth due to the volatile nature of arsenic.

Although the ordered magnetic moment of FeAs is still small, its potential to affect charge transport should be considered. In the isostructural material MnP, noncoplanar magnetic components were suggested to induce a topological anomalous Hall effect in addition to the conventional anomalous Hall effect [33]. One might speculate that in FeAs a field-induced small canted moment deviating from the spin-spiral order provides a noncoplanar spin component which possibly results in a nontrivial coupling between spin and charge. Moreover, a lack of inversion symmetry in the spin degree of freedom introduced by the spin-spiral order could affect the charge transport in an unusual manner. In particular, our two-carrier model description should be reexamined with respect to these effects to see if they play a role in the nonlinear field dependence of ρ_{xy}.

IV. CONCLUSION

In summary, we have presented the unusual magnetotransport properties of a FeAs single crystal below $T_N = 69$ K, where the magnetic order is presented. The nonlinear Hall resistivity feature was analyzed based on the two-carrier model, and it suggests that a minor hole carrier additionally emerges from the magnetic order. The linear MR in the high fields was discussed in relation to the reconstructed Fermi surface which may introduce the linearly dispersive Dirac cone or the strong velocity change in the orbital motion of the electron. However, our observation does not agree with these explanations associated with the intrinsic electronic character. While a spatial inhomogeneity in the carrier mobility may account for the linear MR, an alternative description which uses the spiral magnetic order cannot be ruled out in the full rationalization of the unusual magnetotransport properties of FeAs.

ACKNOWLEDGMENTS

The authors thank S.-L. Drechsler for fruitful discussions and J. Werner for technical support. This work has been supported by the Deutsche Forschungsgemeinschaft through the Priority Programme SPP1458 (Grant No. BU887/15-1) and through the Emmy Noether Programme under Projects No. WU595/3-1 and No. WU595/3-2 (S.W.).

[1] I. Dzyaloshinsky, J. Phys. Chem. Solids **4**, 241 (1958).
[2] T. Moriya, Phys. Rev. **120**, 91 (1960).
[3] A. Neubauer, C. Pfleiderer, B. Binz, A. Rosch, R. Ritz, P. G. Niklowitz, and P. Böni, Phys. Rev. Lett. **102**, 186602 (2009).
[4] S. Mühlbauer, B. Binz, F. Jonietz, C. Pfleiderer, A. Rosch, A. Neubauer, R. Georgii, and P. Böni, Science **323**, 915 (2009).
[5] E. E. Huber and D. H. Ridgley, Phys. Rev. **135**, A1033 (1964).
[6] H. Watanabe, N. Kazama, Y. Yamaguchi, and M. Ohashi, J. Appl. Phys. **40**, 1128 (1969).
[7] K. Selte, A. Kjekshus, W. E. Jamison, A. F. Andresen, and J. E. Engebretsen, Acta Chem. Scand. **25**, 1703 (1971).
[8] A. K. Kari Selte and A. F. Andresen, Acta Chem. Scand. **26**, 3101 (1972).
[9] B. Saparov, J. E. Mitchell, and A. S. Sefat, Supercond. Sci. Technol. **25**, 084016 (2012).
[10] H. Kotegawa, S. Nakahara, H. Tou, and H. Sugawara, J. Phys. Soc. Jpn. **83**, 093702 (2014).
[11] W. Wu, J. Cheng, K. Matsubayashi, P. Kong, F. Lin, C. Jin, N. Wang, Y. Uwatoko, and J. Luo, Nat. Commun. **5**, 5508 (2014).
[12] J.-G. Cheng, K. Matsubayashi, W. Wu, J. P. Sun, F. K. Lin, J. L. Luo, and Y. Uwatoko, Phys. Rev. Lett. **114**, 117001 (2015).
[13] S. Sachdev and B. Keimer, Phys. Today **64**, 29 (2011).
[14] L. Keller, J. S. White, M. Frontzek, P. Babkevich, M. A. Susner, Z. C. Sims, A. S. Sefat, H. M. Rønnow, and C. Rüegg, Phys. Rev. B **91**, 020409 (2015).
[15] H. Kotegawa, S. Nakahara, R. Akamatsu, H. Tou, H. Sugawara, and H. Harima, Phys. Rev. Lett. **114**, 117002 (2015).
[16] J. R. Jeffries, N. P. Butch, H. Cynn, S. R. Saha, K. Kirshenbaum, S. T. Weir, Y. K. Vohra, and J. Paglione, Phys. Rev. B **83**, 134520 (2011).
[17] E. E. Rodriguez, C. Stock, K. L. Krycka, C. F. Majkrzak, P. Zajdel, K. Kirshenbaum, N. P. Butch, S. R. Saha, J. Paglione, and M. A. Green, Phys. Rev. B **83**, 134438 (2011).
[18] K. Segawa and Y. Ando, J. Phys. Soc. Jpn. **78**, 104720 (2009).
[19] D. Gonzalez-Alvarez, F. Grønvold, B. Falk, E. F. Westrum, Jr., R. Blachnik, and G. Kudermann, J. Chem. Thermodyn. **21**, 363 (1989).
[20] D. Parker and I. I. Mazin, Phys. Rev. B **83**, 180403 (2011).
[21] I. Pallecchi, F. Bernardini, M. Tropeano, A. Palenzona, A. Martinelli, C. Ferdeghini, M. Vignolo, S. Massidda, and M. Putti, Phys. Rev. B **84**, 134524 (2011).
[22] H.-H. Kuo, J.-H. Chu, S. C. Riggs, L. Yu, P. L. McMahon, K. De Greve, Y. Yamamoto, J. G. Analytis, and I. R. Fisher, Phys. Rev. B **84**, 054540 (2011).
[23] D. A. Moseley, K. A. Yates, N. Peng, D. Mandrus, A. S. Sefat, W. R. Branford, and L. F. Cohen, Phys. Rev. B **91**, 054512 (2015).
[24] A. A. Abrikosov, Phys. Rev. B **58**, 2788 (1998).
[25] P. Richard, K. Nakayama, T. Sato, M. Neupane, Y.-M. Xu, J. H. Bowen, G. F. Chen, J. L. Luo, N. L. Wang, X. Dai *et al.*, Phys. Rev. Lett. **104**, 137001 (2010).
[26] S. Ishida, T. Liang, M. Nakajima, K. Kihou, C. H. Lee, A. Iyo, H. Eisaki, T. Kakeshita, T. Kida, M. Hagiwara *et al.*, Phys. Rev. B **84**, 184514 (2011).
[27] K. K. Huynh, Y. Tanabe, and K. Tanigaki, Phys. Rev. Lett. **106**, 217004 (2011).
[28] A. E. Koshelev, Phys. Rev. B **88**, 060412 (2013).
[29] R. Xu, A. Husmann, T. F. Rosenbaum, M.-L. Saboungi, J. E. Enderby, and P. B. Littlewood, Nature (London) **390**, 57 (1997).
[30] N. Kozlova, N. Mori, O. Makarovsky, L. Eaves, Q. Zhuang, A. Krier, and A. Patanè, Nat. Commun. **3**, 1097 (2012).
[31] Z. Hou, B. Yang, Y. Wang, B. Ding, X. Zhang, Y. Yao, E. Liu, X. Xi, G. Wu, Z. Zeng *et al.*, Sci. Rep. **6**, 23807 (2016).
[32] A. Narayanan, M. D. Watson, S. F. Blake, N. Bruyant, L. Drigo, Y. L. Chen, D. Prabhakaran, B. Yan, C. Felser, T. Kong *et al.*, Phys. Rev. Lett. **114**, 117201 (2015).
[33] Y. Shiomi, S. Iguchi, and Y. Tokura, Phys. Rev. B **86**, 180404 (2012).